Matter-wave diffraction approaching limits predicted by Feynman path integrals for multipath interference

A. Ronny Barnea,* Ori Cheshnovsky, and Uzi Even
School of Chemistry, Sackler Faculty of Exact Sciences, Tel Aviv University, Tel Aviv 69978, Israel

(Received 8 October 2017; published 1 February 2018)

Interference experiments have been paramount in our understanding of quantum mechanics and are frequently the basis of testing the superposition principle in the framework of quantum theory. In recent years, several studies have challenged the nature of wave-function interference from the perspective of Born's rule—namely, the manifestation of so-called high-order interference terms in a superposition generated by diffraction of the wave functions. Here we present an experimental test of multipath interference in the diffraction of metastable helium atoms, with large-number counting statistics, comparable to photon-based experiments. We use a variation of the original triple-slit experiment and accurate single-event counting techniques to provide a new experimental bound of 2.9×10^{-5} on the statistical deviation from the commonly approximated null third-order interference term in Born's rule for matter waves. Our value is on the order of the maximal contribution predicted for multipath trajectories by Feynman path integrals.

DOI: 10.1103/PhysRevA.97.023601

I. INTRODUCTION

Quantum mechanics and the superposition principle are cornerstones of our understanding of physical systems, and have been targeted numerously by theoretical and experimental studies. Since Young's double-slit experiment [1] in 1801, diffraction experiments have been crucial in asserting the superposition concept, and testing interference of wave functions. The quantum nature of particles and their interference is considered theoretically throughout the literature [2–14]. Interference from double- and triple-slit experiments, as well as diffraction gratings were notably tested with photons [15–22], electrons [23–25], neutrons [26], atoms [27–32], clusters [33–36], and even large molecules [37–42].

Interference measurement is readily treated within the framework of Born's rule [43], which at its simplest states $P_{(\boldsymbol{r},t)} = |\psi_{(\boldsymbol{r},t)}|^2$, with $P_{(\boldsymbol{r},t)}$ the probability to find a particle, defined by a wave function $\psi_{(\boldsymbol{r},t)}$. This should hold true for any arbitrary initial wave function and for any superposition of these, emitted, e.g., from N slits (separated by a distance d). Considering multiple paths, e.g., in a double-slit experiment, the probability may be written as $P_{AB} = |\psi_A + \psi_B|^2 = P_A + P_B + I_{AB}$. Here ψ_A, ψ_B represent the wave functions when slits A or B are open, respectively, and P_A, P_B are the probabilities to detect the particle originating from the corresponding slit. $I_{AB} = \psi_A^* \psi_B + \psi_A \psi_B^*$, is the interference term of two slits. The position and time arguments are omitted henceforth for brevity. An analogous term may be written for triple-slit interference:

$$I_{ABC} = P_{ABC} - P_{AB} - P_{BC} - P_{AC} + P_A + P_B + P_C. \quad (1)$$

The probability can be defined considering interference only from pairs of slits, if the third-order interference term [from interaction of three slits—left-hand side of Eq. (1)] is zero. This is regularly approximated in quantum mechanics and Born's rule. Nullification of third-order interference also annuls higher-order interferences as suggested by Sorkin [2]. Deviation from zero would mean particles traverse multiple slits before being detected, invalidating a wave function limited to superposition of second-order interferences. That case is dealt within the formalism of Feynman path integrals [44]. We denote the deviation of third-(or higher-) order interference from zero, for three identical slits, by the so-called Sorkin parameter:

$$\epsilon = P_{111} - P_{110} - P_{011} - P_{101} + P_{100} + P_{010} + P_{001}. \quad (2)$$

This parameter is in essence a measure of how complete our description of the quantum dynamics taking place in the experiment is, in the framework of Born's rule. Interactions beyond the customary squaring of amplitudes which result in finite probabilities will manifest themselves as a nonzero Sorkin parameter [2]. We define the probabilities with ones and zeros, stating if a slit is open or closed. This notation will be used throughout the paper.

Recently, a significant deviation was observed using photons, by tailoring their near-field interactions with adjacent slits, yielding conditions favorable for high-order interference [22]. This calls for broader treatment of the problem, even for experimentally achievable conditions, and at any rate motivates further, meticulous exploration of the phenomenon. Cotter *et al.* recently investigated possible multipath interference using matter waves for the first time [45]. Their experiment was statistically limited due to the low throughput of their setup, and the use of particles of high mass (with small de Broglie wavelength) originating from a thermal source (with a wide velocity distribution) led to limited coherence of the particle beam. A more thorough test using cold, low-mass species with high coherence, and considerably better statistics, constitutes an important advancement for testing the limits of accepted quantum theory.

In this work, we test multipath interference with matter waves using a highly coherent metastable-helium-atom (1S2S)

*Corresponding author: ronnybar@mail.tau.ac.il

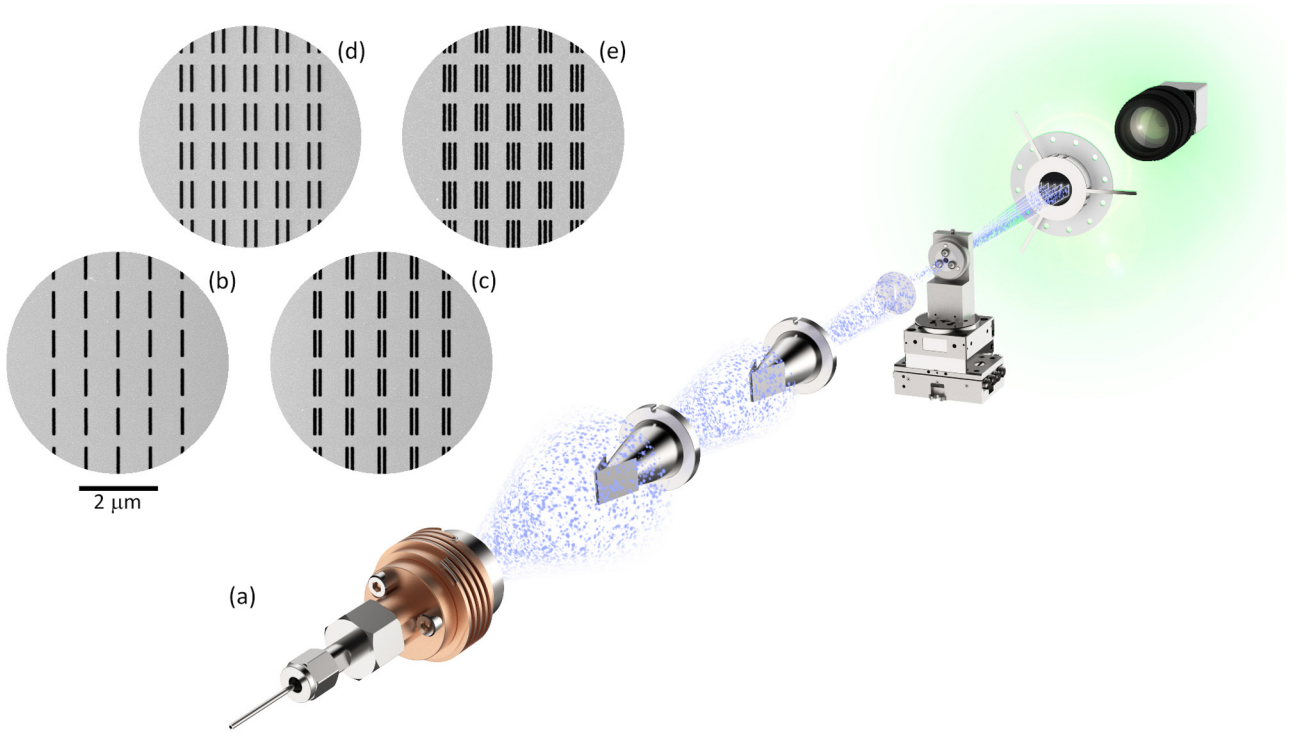

FIG. 1. Schematic view of the experimental setup. (a) The He* beam is generated in a high-vacuum chamber at an Even-Lavie pulsed-valve source, using dielectric-barrier discharge, and collimated by two skimmers and a movable slit. The beam then interacts with the configuration of the mask chosen using nanopositioning stages. The diffracted metastable atoms are detected as they hit an MCP phosphor assembly. The emitted bursts of light generated from impacts of single atoms are imaged by a CMOS camera. Real-time analysis yields localized single-event counting and is accumulated over time to form each diffraction pattern. (b–e) Environmental scanning electron microscope images (20 000×) showing the four different mask configurations—100, 110, 101, 111, correspondingly. These patterns repeat over roughly 1.6 mm in height.

beam in a triple-slit experiment variant, involving direct detection of individual atoms as they are diffracted, and comprising over 10^6 counts—statistically comparable to previous photon-based experiments.

II. EXPERIMENTAL REALIZATION

The interference of our matter waves is produced using a thin nanofabricated mask (50-nm amorphous silicon nitride membrane) patterned with slits of opening $a = 84.5 \pm 0.3$ nm and spacing $d = 136.5 \pm 0.6$ nm (covering a height of roughly 1.6 mm), comprising the various open and closed configurations available with a triple-slit setup, i.e., a single slit, double slit, double slit separated by two periods ($2d$), and triple slit. Each configuration in our mask is repeated consecutively five times (see Fig. 1 and Supplemental Material [46]) to increase the throughput fivefold, while maintaining distinctive diffraction patterns. Care was taken to deal with possible long-range interference between multiple instances. This issue is later addressed in length. Since all three of the single-slit configurations would yield the same diffraction pattern (up to an undetectable translation), only one single-slit configuration is required. Similarly, the two double-slit configurations are reduced to a single configuration as well. Thus, our mask includes four configurations in total, denoted 100, 110, 101, and 111, for the single, double-, spaced double, and triple slit, respectively (see also Fig. S1 [46]). Since we use an excited, metastable state of helium atoms, any interaction with a surface causes relaxation and decay to the ground state, leaving little (if any) diffusively scattered excited (detectable) particles in the vacuum. Our measurement is therefore virtually background free.

We have used a highly collimated (FWHM ≈ 100 μrad, speed ratio ≈ 45) beam of metastable helium (He*), generated in a high-vacuum chamber ($P < 10^{-7}$ mbar) by a pulsed Even-Lavie valve [47] and a dielectric-barrier discharge source [48] which has been modified for greater yield, pulse-to-pulse repeatability, and stability over time (using microfabricated metallic foils that enhance the electric field). The beam, traveling at $v = 1760 \pm 40$ m/s, is collimated by a 20-μm skimmer and a 20-μm movable slit, positioned approximately 250 and 850 mm, correspondingly, downstream from the nozzle (with an intermediate wider skimmer filtering wide-angle atoms before entrance to the interaction chamber). The atoms then undergo diffraction at the mask which is uniformly ($\pm 0.2\%$) illuminated by the beam (verified by mapping the intensity distribution of the total transmitted flux with translation of the mask across the beam). The mask is accurately positioned by linear and rotational nanopositioning stages ($\sim$60 mm away from the collimation slit). Following the diffraction the atoms continue in free flight for about 800 mm to impact a microchannel plate (MCP) phosphor assembly. The light emitted by each impact is imaged through an optical window by a complementary metal-oxide semiconductor (CMOS) camera mounted outside of the vacuum chamber. The signal is transmitted to a PC and undergoes localization and analysis in real time. The experimental setup is depicted in Fig. 1.

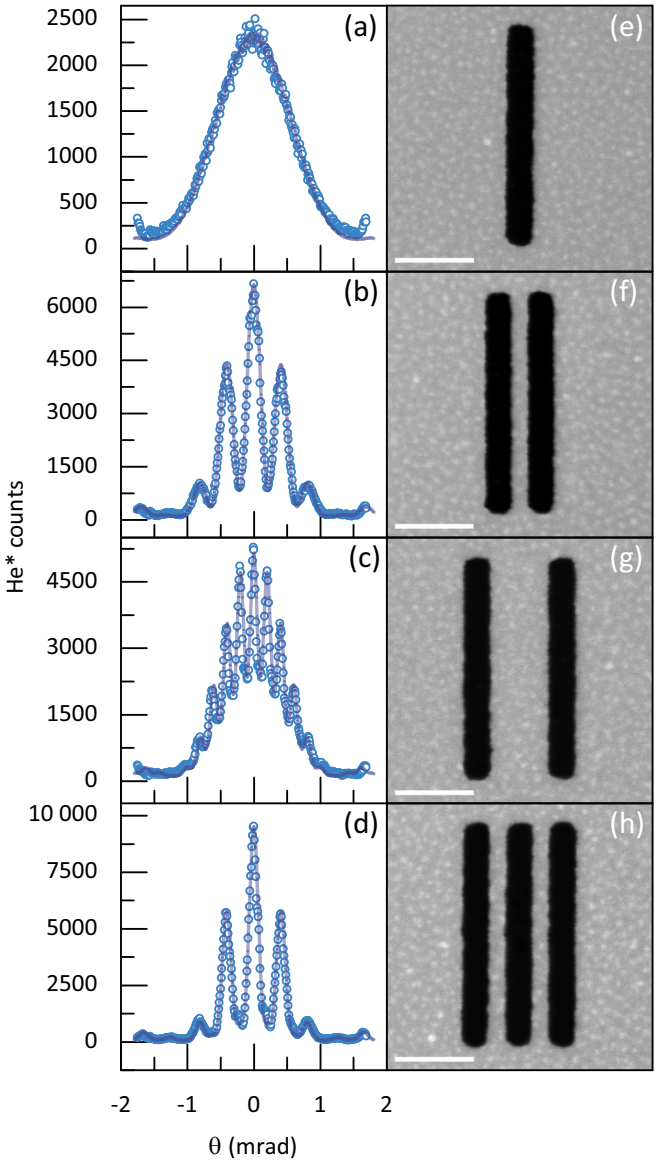

FIG. 2. Diffraction of the He* beam through the four configurations of the mask. (a–d) Counts of He* acquired (from top to bottom) in diffraction from the 100 (single-slit), 110 (double-slit), 101 (spaced double-slit), and 111 (triple-slit) configurations, respectively. Each data set is fitted (dark solid lines) to the model in Eq. (4) by means of least squares. (e–h) Environmental scanning electron microscope images (130 000×) of slits in the corresponding configurations. The scale bars are 250 nm.

The experiment was conducted during roughly 48 h with the system operating at 40 Hz, yielding (on average) one diffraction event for every four pulses. In total, 1.7×10^6 counts of He* were collected to yield four unique diffraction patterns (see Fig. 2). The data were fitted (least squares) to an analytical model of the diffraction, considering the superposition of wave fronts with finite angular dispersion, emitted from each of the slits in the experiment.

$$\Psi = \sum_j \psi_j = \sum_j \left[e^{-ikjd\theta} \frac{2\sin\left(k\theta\frac{a}{2}\right)}{k\theta} \right]. \tag{3}$$

ψ_j is the wave function emitted from the jth slit, Ψ the superposition on the screen, and the summation is over indices where the slits are open. k, d, a, and θ represent the momentum of the atom in the beam ($\frac{2\pi}{\lambda_{\mathrm{dB}}}$), the period (distance between adjacent slits), the effective [49] width of the slits, and the angle of detection, respectively. λ_{dB} is the de Broglie wavelength. Two additional terms are introduced: one accounting for the angular dispersion of the beam, $\Delta\theta$ (expressed as a convolution with a Gaussian function); and the other representing random variations in the edges of the slits (σ_a), yielding different effective widths on entrance and exit from the mask [32]. The possible diffraction from the collimation stage (<3 μrad) is ignored here since it is much smaller than $\Delta\theta$. We thus have the expected interference pattern:

$$\mathrm{I}_{\Psi\mathrm{model}} = (|\Psi|^2 * e^{-\frac{\theta^2}{2\Delta\theta^2}})\, e^{-\frac{(k\theta\sigma_a)^2}{4}}. \tag{4}$$

The asterisk denotes the convolution. We note here that while this model is used to fit the diffraction data of each of the configurations and help validate our understanding of the physical setup, it is unused in the statistical analysis aiming to deal with multipath interference and calculation of the Sorkin parameter (given in the next section). Considering the aforementioned and the good fit of our experimental data to the analytical model (see Fig. 2), we refrain from treating the full problem of the metastable atoms passing through the slits in the silicon nitride membranes—the accumulation of phase across the slits and edge effects (including deexcitation), and stick to the "effective slit" approach [49].

III. MULTIPATH INTERFERENCE TEST WITH BORN'S RULE

If the sum rule of probabilities to detect each wave function is true, then it should be so for every position on the screen. We can therefore treat all measurement positions (on the diffraction axis) as separate tests, and attempt to validate the nullification of the high-order interference term (originating from multiple interacting paths) in each individually, as well as by looking at the statistical outcome of all the data. Every point in the data set represents a channel, corresponding to a horizontal camera pixel (~8 μm on the phosphor screen) and is composed of an integral over all vertical pixels. Each channel of the acquired diffraction pattern is transformed into detection probability using $P_i^k = \frac{I_i^k}{\sum_k I_i^k}$, where I_i^k represents the number of counts in the kth channel of the ith configuration (100, 110, 101, or 111). Our test is obtained by overlaying the probability-transformed diffraction patterns and calculating the appropriate linear combination to yield the Sorkin parameter. Accounting for the reduced number of configurations in the experiment (four instead of seven), Eq. (2) can be transformed into $\epsilon = P_{111} - 2P_{110} - P_{101} + 3P_{100}$. Keep in mind that this is given for the case of illumination of all configurations simultaneously, by the same flux. Since our experiment probes each configuration separately and considers only the collected counts (rather than total incident flux), we must take into account the relative fluxes of the different configurations, i.e., a factor of 2/3 for the 110 and 101 configurations, and a factor

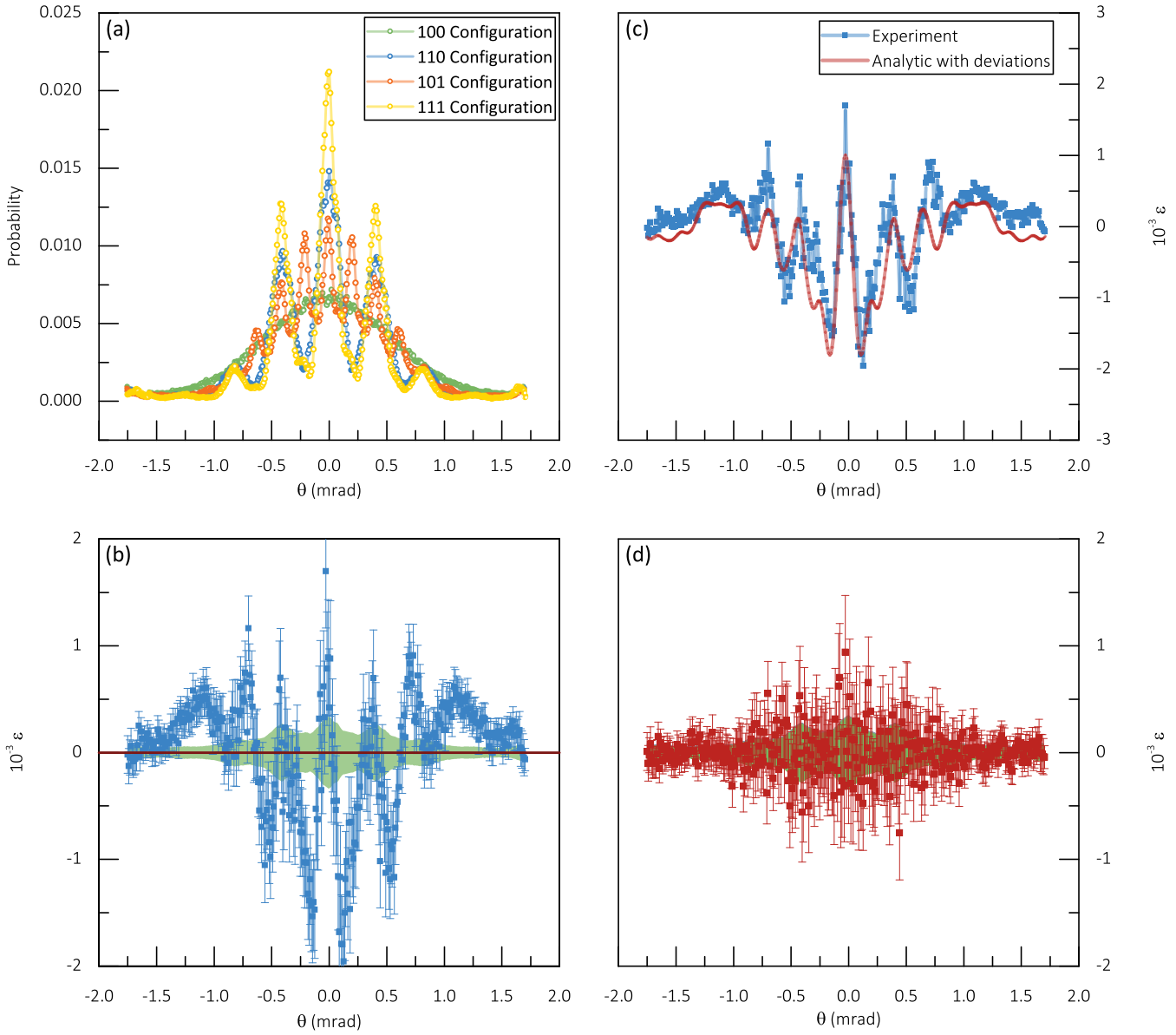

FIG. 3. Test of multipath interference of He* in the modified triple-slit experiment. (a) The diffraction patterns measured for the slits configurations: 100 (green), 110 (blue), 101 (red), and 111 (yellow). (b) The Sorkin parameter deduced from Eq. (5). The red line represents the mean, which is practically zero. The green colored area stands for the shot noise (proportional to the square root of the number of collected counts). The error bars are the probability errors arising from finite statistics. The standard deviation for the Sorkin parameter is $\epsilon_\sigma = 5.4 \times 10^{-4}$. Considering each channel as a separate experiment sets an upper bound on the statistical deviation of $|\epsilon| \leqslant 2.9 \times 10^{-5}$. The oscillations apparent in (b) arise from imperfections in the mask—generating systematic errors which are observable due to our highly accurate measurements. (c) The Sorkin parameter overlaid by an analytical calculation using Eq. (4)—plugging in the appropriate parameters d and a derived from our image-processing-based analysis of the mask (see Fig. S3 [46]). (d) The Sorkin parameter following a Fourier filter (removing frequencies rising above 5σ of the noise level)—basically eliminating fabrication-related, periodic systematic errors in the measurement. The quantitative outcome this filtering yields is not considered as the main result of the paper. However, it does give an idea of how the results would have looked, given no fabrication errors. The scale is kept identical to (b) for clarity.

of 1/3 for the 100 configuration. We thus get

$$\epsilon^k = P^k_{111} - \tfrac{4}{3}P^k_{110} - \tfrac{2}{3}P^k_{101} + P^k_{100}, \tag{5}$$

with k being the measurement channel on the diffraction axis.

Figure 3 shows our experiment clearly validates the null approximation for multipath interference with matter waves, in our case of de Broglie wavelength $\lambda_{\mathrm{dB}} \approx 56$ pm. The Sorkin parameter mean over all channels is practically zero and its uncertainty is taken as the standard deviation divided by the square root of the number of experiments (360 measurement channels), $\frac{\epsilon_\sigma}{\sqrt{N}}$ which puts a new upper bound on the deviation at $|\epsilon| \leqslant 2.9 \times 10^{-5}$. In previous papers discussing Born's rule and testing the existence of high-order interference,

TABLE I. Comparison of this work with previous experimental studies considering normalized Sorkin parameters.

Parameter	Sinha *et al.* (2009) [19]	Sinha *et al.* (2010) [20]	Söllner *et al.* (2012) [21]	This work
ρ	$(1.0 \pm 0.1) \times 10^{-2}$[a]	$(0.6 \pm 1.2) \times 10^{-2}$[a]	$(-1.5 \pm 2.9) \times 10^{-3}$[b]	$(2.9 \pm 0.4) \times 10^{-2}$
	Magaña-Loaiza *et al.* (2016) [22]	This work		
κ_1	$(9.7 \pm 3.2) \times 10^{-3}$[c]	$\leqslant 3 \times 10^{-9}$		
	Cotter *et al.* (2017) [45]			
κ_2	$\leqslant 10^{-2}$	$\leqslant 1.4 \times 10^{-4}$		

[a]Only a single position in the diffraction was considered.
[b]Only the maximum of the central peak was considered. The result with best statistics (over an order of magnitude difference) in the published paper is $\rho = (-1.4 \pm 0.1) \times 10^{-2}$.
[c]The data were graphically extracted from the published paper, for the configuration favoring no multipath interference.

different estimates were used to gauge the results. Namely, a normalized Sorkin parameter (usually denoted κ) was used, with the normalization varying among authors. Since these are not consistent and are difficult to compare, we refrain from using these forms in our analysis and stick to the more general Sorkin parameter ϵ. A representation of an equivalent Sorkin parameter, considering counts instead of probabilities, is shown in Fig. S2 [46].

IV. COMPARISON WITH PREVIOUS WORK

Our results are compared with the normalized Sorkin parameters ρ and κ defined in previous work as

$$\rho = \frac{\epsilon}{|P_{110} - P_{100} - P_{010}| + |P_{011} - P_{010} - P_{001}| + |P_{101} - P_{100} - P_{001}|}, \tag{6}$$

$$\kappa_1 = \frac{\epsilon}{I_{\max}}, \tag{7}$$

$$\kappa_2 = \frac{\epsilon_{\text{counts}}}{I_{\text{total}}}, \tag{8}$$

where ϵ_{counts} is the same linear combination as ϵ, using counts instead of probabilities, $I_{\max}$ is the maximal number of counts (i.e., in the central diffraction peak), and I_{total} is the sum of all collected counts. We use $P_{100} = P_{010} = P_{001}$ to conform to our setup. Table I shows a comparison of our work with several previously published ones, with respect to the accuracy of the test of Born's rule in nullifying high-order interference. Since not enough data are provided regarding the previous experiments, the comparison with each is kept within its own reference.

V. LONG-RANGE INTERFERENCE—COHERENCE OF THE He* BEAM

The geometry of our mask (five equivalent groups) supports a possibility for coherent interference between slits which lie outside of their own group. This means that slits from different instances of the basic triple-slit configuration, positioned farther than one or two slit spacings apart, may contribute to the superposition such that they change the observed pattern on the screen, rather than just add to the flux. We use analytic calculations to compare the expected interference patterns for a varying number of interfering groups of slits and find that coherent interference takes place only between pairs of adjacent groups, and no farther. The effect is captured in the subfeatures apparent in the diffraction patterns as shown in Fig. 4.

By taking the fast Fourier transform of the diffraction patterns it is clear that a single peak rises above the noise level for the case of the single slit (100 configuration)—whereas if no long-range interference existed, i.e., different groups of the mask would not interact, there should be no peaks in the momentum spectrum [see Fig. 4(c)]. Similarly, for the case of the double-slit (110), a first strong peak represents the interference between the two adjacent slits in the double-slit configuration (separated by distance d), while three additional peaks appear at the corresponding harmonics (five, six, and seven periods), arising from the interference with the neighboring double-slit group in the mask [see Fig. 4(d)]. This is consistent with the description of transverse coherence length for matter waves $l_{\text{coherence}} = \frac{\lambda_{\text{dB}}}{2\,\alpha}$ (α being the angle between the effective source and the interaction region) [50], which for our beam is approximately 820 nm—very close to the distance between repeating groups of slits in our mask ($6d = 810$ nm $\approx 0.988\, l_{\text{coherence}}$). The decay in amplitude for increasing harmonics in Fig. 4(d) can be explained by this as well, with the rightmost peak corresponding already to a situation of interaction significantly beyond $l_{\text{coherence}}$, and thus is prominently suppressed. Notice that no additional peaks appear in the spectrum, suggesting indeed that coherent interference takes place only between pairs of neighboring groups, and does not include slits from groups situated farther. The analysis also reveals the interactions' strength over distance in the form of relative intensities of the peaks in Fig. 4(d). The

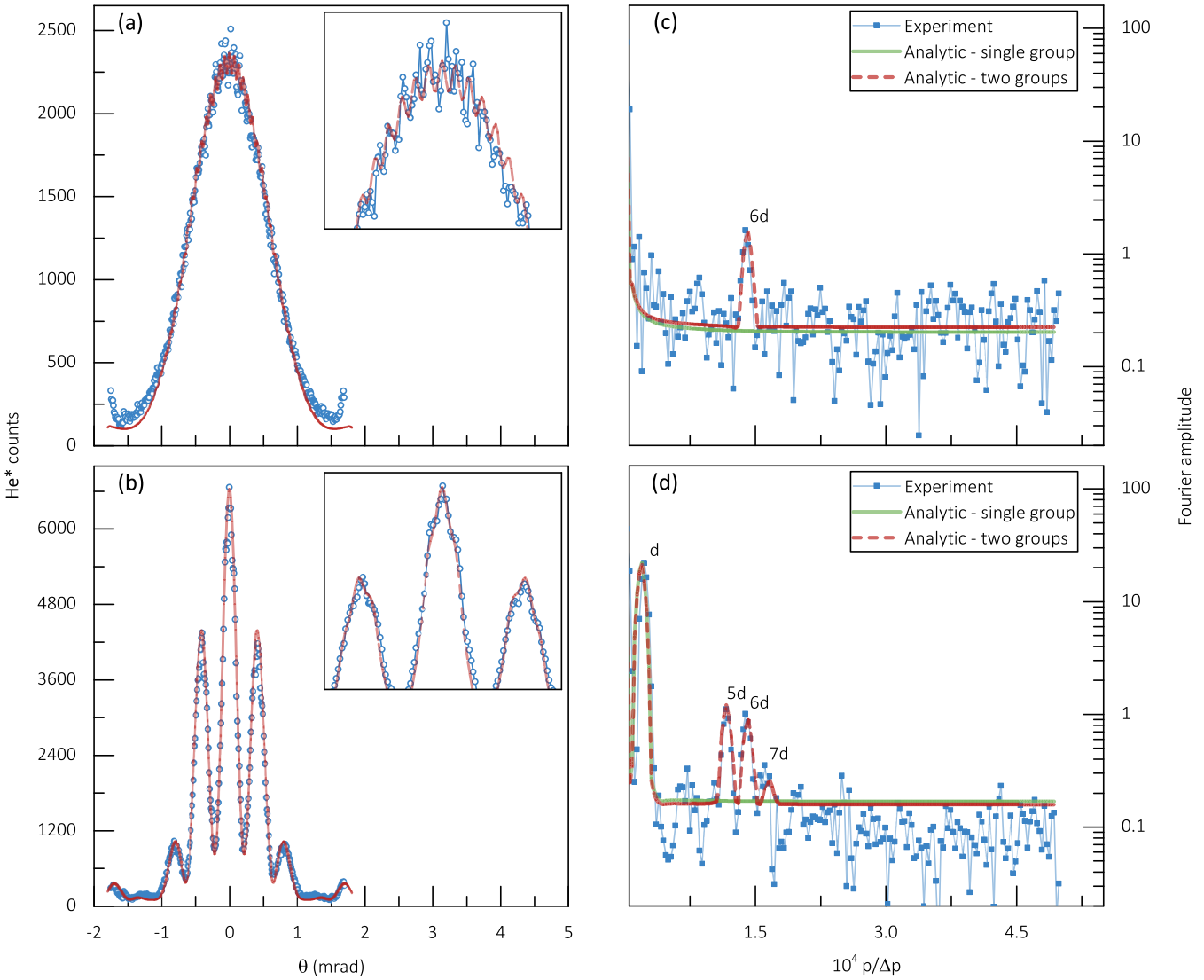

FIG. 4. Long-range coherent interference of the He* beam. (a,b) The experimentally measured diffraction patterns for the 100 and 110 configurations, respectively, fitted (red lines) to the analytical model in Eq. (4), considering two groups of interacting slits. The insets in (a,b) show blowups emphasizing the subfeatures apparent in the diffraction—a product of interference between two instances of each configuration. (c,d) Fast Fourier transforms comparing the experimental peaks in the spectra with the analytical model, for a single group (green line) and for two instances of the same configuration (red dashed line). The labels in (c,d) note the corresponding distances between interacting slits. Constant spectral noise was added to the analytical computations for convenient comparison to the experimental data.

interferences between slits spaced $5d$ and $6d$ from each other contribute approximately 5% of the double-slit interference to the overall diffraction pattern, while the slits spaced $7d$ from each other only contribute roughly 1.5%.

VI. DISCUSSION

We have tested multipath interference of matter waves using accurate particle-counting methods and large-number statistics, investigating many data channels, making our experiment comparable to previous experiments with photons. We put a new experimental upper bound on the possible contributions of third- (and higher-) order interference, originating from multipath trajectories, for massive particles (evaluated by the Sorkin parameter) of $|\epsilon| \leqslant 2.9 \times 10^{-5}$. This value is fairly close to the maximal contribution of multipath interference predicted by Feynman path integrals which is roughly on the order of 10^{-5} for our experimental conditions [10,11]. Crossing that threshold in a matter-wave diffraction experiment can serve to validate or challenge the formalism used in diffraction and in particular quantum diffraction and Feynman path integrals. This may have ramifications on our perception of matter waves and their interactions at diffracting media, and as such is of major significance. However, procuring the necessary experimental data would be extremely difficult. Even in the best case scenario, not accounting for any new problems which may arise at greater accuracy, as the error scales like the square root of the number of counts, one will need to increase the collection time more than tenfold (around one month or so in our experimental setup), a feat that will surely demand extensive infrastructural and systematic improvements. We suggest that similar experimental studies in the future use

the basic ϵ parameter as reference, which will also aid in comparing various works in the field. The oscillations apparent in Fig. 3(b) are attributed to geometrical inaccuracy (width and spacing) of the mask's slits, arising from finite resolution in the lithography process (see Supplemental Material [46]). Our analysis (see Fig. S3 [46]), based on image processing of the mask, revealed a deviation between the various configurations of $d_\sigma = 0.7\%$ in the spacing of the slits and $a_\sigma = 2\%$ in the widths of the slits, which by plugging in Eq. (4) and recalculating ϵ using Eq. (5) yields a result correlating quite well to our data and, nevertheless, serves to qualitatively explain the observed systematic errors in our experiment (see Fig. 3(c) and Fig. S4 [46]). Note that these errors are observable due to the high signal-to-noise ratio in our experiment. This concept is further demonstrated in Fig. S5 [46], in which ϵ is calculated using Eq. (5) for different deviations in the period d of the triple-slit configuration. An analysis of our results following a Fourier filter, which basically eliminates periodic systematic errors, stemming from imperfections in the mask, is presented in Fig. 3(d).

Our test with multiple slit configurations demonstrates the validity of the theory for more complicated scenarios than the original triple-slit experiment, and is consistent with models for coherence of matter waves. Further testing configurations of growing complexity, with an ability to dynamically tune the level of interference of wave functions, may serve as a good testing ground for exploring the limits of the validity of Born's rule and standard quantum mechanics for matter waves.

ACKNOWLEDGMENTS

The authors thank the staff of Tel Aviv University's Mechanical Workshop for Research and Development for their help with the design and machining of parts of the experimental setup. We thank Z. Barkay for her assistance in characterization of the diffraction mask, and C. Brand and M. Arndt for helpful discussions. This work was partially supported by the Israel Science Foundation (Grant No. 1716/13).

[1] T. Young, *A Course of Lectures on Natural Philosophy and the Mechanical Arts* (J. Johnson, London, 1807), p. 892.
[2] R. D. Sorkin, Mod. Phys. Lett. **9**, 3119 (1994).
[3] M. O. Scully, B. G. Englert, and H. Walther, Nature **351**, 111 (1991).
[4] W. H. Zurek, Phys. Rev. A **71**, 052105 (2005).
[5] S. L. Adler and A. Bassi, Science **325**, 275 (2009).
[6] C. Ududec, H. Barnum, and J. Emerson, Found. Phys. **41**, 396 (2011).
[7] A. Khrennikov, in *Advances in Quantum Theory—2010, Växjö, Sweden*, Proceedings of the International Conference on Advances in Quantum Theory, AIP Conf. Proc. No. 1327, edited by G. Jaeger, A. Khrennikov, M. Schlosshauer, and G. Weihs (AIP, New York, 2011), p. 387.
[8] H. De Raedt, K. Michielsen, and K. Hess, Phys. Rev. A **85**, 012101 (2012).
[9] M. F. Pusey, J. Barrett, and T. Rudolph, Nat. Phys. **8**, 475 (2012).
[10] R. Sawant, J. Samuel, A. Sinha, S. Sinha, and U. Sinha, Phys. Rev. Lett. **113**, 120406 (2014).
[11] A. Sinha, A. H. Vijay, and U. Sinha, Sci. Rep. **5**, 10304 (2015).
[12] M. Ringbauer, B. Duffus, C. Branciard, E. G. Cavalcanti, A. G. White, and A. Fedrizzi, Nat. Phys. **11**, 249 (2015).
[13] D. K. Park, O. Moussa, and R. Laflamme, New J. Phys. **14**, 113025 (2012).
[14] X. Y. Wu, H. Li, B. J. Zhang, J. Ma, X. J. Liu, N. Ba, H. Dong, S. Q. Zhang, J. Wang, Y. H. Wu, and X. G. Yin, arXiv:1305.2416v1.
[15] S. Kocsis, B. Braverman, S. Ravets, M. J. Stevens, R. P. Mirin, L. K. Shalm, and A. M. Steinberg, Science **332**, 1170 (2011).
[16] J. M. Hickmann, E. J. S. Fonseca, and A. J. Jesus-Silva, Europhys. Lett. **96**, 64006 (2011).
[17] R. Menzel, D. Puhlmann, A. Heuer, and W. P. Schleich, Proc. Natl. Acad. Sci. USA **109**, 9314 (2012).
[18] V. Jacques, E. Wu, T. Toury, F. Treussart, A. Aspect, P. Grangier, and J. F. Roch, Eur. Phys. J. D **35**, 561 (2005).
[19] U. Sinha, C. Couteau, Z. Medendorp, I. Söllner, R. Laflamme, R. Sorkin, and G. Weihs, in *Foundations of Probability and Physics–5—2008, Växjö, Sweden*, AIP Conf. Proc. No. 1101, edited by L. Accardi, G. Adenier, G. Fuchs, G. Jaeger, A. Yu. Khrennikov, J.-A. Larsson, and S. Stenholm (AIP, New York, 2009), p. 200.
[20] U. Sinha, C. Couteau, T. Jennewein, R. Laflamme, and G. Weihs, Science **329**, 418 (2010).
[21] I. Söllner, B. Gschösser, P. Mai, B. Pressl, Z. Vörös, and G. Weihs, Found. Phys. **42**, 742 (2012).
[22] O. S. Magaña-Loaiza, I. De Leon, M. Mirhosseini, R. Fickler, A. Safari, U. Mick, B. McIntyre, P. Banzer, B. Rodenburg, G. Leuchs, and R. W. Boyd, Nat. Commun. **7**, 13987 (2016).
[23] A. Ohshita, N. Takayama, and H. Tomita, J. Electron. Microsc. **34**, 357 (1985).
[24] B. J. McMorran and A. D. Cronin, New J. Phys. **11**, 033021 (2009).
[25] R. Bach, D. Pope, S. H. Liou, and H. Batelaan, New J. Phys. **15**, 033018 (2013).
[26] A. Zeilinger, R. Gähler, C. G. Shull, W. Treimer, and W. Mampe, Rev. Mod. Phys. **60**, 1067 (1988).
[27] M. J. Cardillo and G. E. Becker, Phys. Rev. Lett. **40**, 1148 (1978).
[28] D. W. Keith, M. L. Schattenburg, H. I. Smith, and D. E. Pritchard, Phys. Rev. Lett. **61**, 1580 (1988).
[29] O. Carnal and J. Mlynek, Phys. Rev. Lett. **66**, 2689 (1991).
[30] O. Carnal, A. Faulstich, and J. Mlynek, Appl. Phys. B **53**, 88 (1991).
[31] F. Shimizu, K. Shimizu, and H. Takuma, Phys. Rev. A **46**, R17 (1992).
[32] R. E. Grisenti, W. Schöllkopf, J. P. Toennies, J. R. Manson, T. A. Savas, and H. I. Smith, Phys. Rev. A **61**, 033608 (2000).
[33] W. Schollkopf and J. P. Toennies, Science **266**, 1345 (1994).
[34] W. Schöllkopf and J. P. Toennies, J. Chem. Phys. **104**, 1155 (1996).
[35] R. Brühl, R. Guardiola, A. Kalinin, O. Kornilov, J. Navarro, T. Savas, and J. P. Toennies, Phys. Rev. Lett. **92**, 185301 (2004).
[36] O. Kornilov and J. P. Toennies, Europhys. News **38**, 22 (2007).

[37] M. Arndt, O. Nairz, J. Vos-Andreae, C. Keller, G. van der Zouw, and A. Zeilinger, Nature **401**, 680 (1999).
[38] O. Nairz, B. Brezger, M. Arndt, and A. Zeilinger, Phys. Rev. Lett. **87**, 160401 (2001).
[39] O. Nairz, M. Arndt, and A. Zeilinger, Am. J. Phys. **71**, 319 (2003).
[40] S. Gerlich, L. Hackermuller, K. Hornberger, A. Stibor, H. Ulbricht, M. Gring, F. Goldfarb, T. Savas, M. Muri, M. Mayor, and M. Arndt, Nat. Phys. **3**, 711 (2007).
[41] S. Gerlich, S. Eibenberger, M. Tomandl, S. Nimmrichter, K. Hornberger, P. J. Fagan, J. Tüxen, M. Mayor, and M. Arndt, Nat. Commun. **2**, 263 (2011).
[42] C. Brand, M. Sclafani, C. Knobloch, Y. Lilach, T. Juffmann, J. Kotakoski, C. Mangler, A. Winter, A. Turchanin, J. Meyer, O. Cheshnovsky, and M. Arndt, Nat. Nanotechnol. **10**, 845 (2015).
[43] M. Born, Zeit. Phys. **38**, 803 (1927).
[44] R. P. Feynman and A. R. Hibbs, *Quantum Mechanics and Path Integrals* (McGraw-Hill, New York, 1965).
[45] J. P. Cotter, C. Brand, C. Knobloch, Y. Lilach, O. Cheshnovsky, and M. Arndt, Sci. Adv. **3**, e1602478 (2017).
[46] See Supplemental Material at http://link.aps.org/supplemental/10.1103/PhysRevA.97.023601 for details of the diffraction-mask preparation process and signal-acquisition. It also includes figures and data pertaining to analysis of fabrication and systematic errors as well as additional information about the experimental system and the results.
[47] U. Even, Adv. Chem. **2014**, 11 (2014).
[48] K. Luria, N. Lavie, and U. Even, Rev. Sci. Instrum. **80**, 104102 (2009).
[49] R. E. Grisenti, W. Schöllkopf, J. P. Toennies, G. C. Hegerfeldt, and T. Köhler, Phys. Rev. Lett. **83**, 1755 (1999).
[50] C. Keller, J. Schmiedmayer, and A. Zeilinger, Opt. Commun. **179**, 129 (2000).